ACS APPLIED MATERIALS & INTERFACES

Research Article

www.acsami.org

Facile Fabrication of Three-Dimensional Graphene Foam/Poly(dimethylsiloxane) Composites and Their Potential Application as Strain Sensor

Rongqing Xu,[†] Yunqing Lu,[‡] Chunhui Jiang,[†] Jing Chen,*[,†] Peng Mao,[§] Guanghua Gao,[†] Labao Zhang,[§] and Shan Wu[§]

[†]College of Electronic Science and Engineering and [‡]School of Optoelectronic Engineering, Nanjing University of Posts and Telecommunications, Nanjing 210046, China

[§]National Laboratory of Solid State Microstructures, Nanjing University, Nanjing 210093, China

ABSTRACT: A three-dimensional (3D) graphene foam (GF)/poly(dimethylsiloxane) (PDMS) composite was fabricated by infiltrating PDMS into 3D GF, which was synthesized by chemical vapor deposition (CVD) with nickel foam as template. The electrical properties of the GF/PDMS composite under bending stress were investigated, indicating the resistance of the GF/PDMS composite was increased with the bending curvature. To improve the bending sensitivity of the GF/PDMS composite, a thin layer of poly(ethylene terephthalate) (PET) was introduced as substrate to form double-layer GF/PDMS−PET composite, whose measurements showed that the resistance of the GF/PDMS−PET composite was still increased when bended to the side of PET, whereas its resistance would be decreased when bended to the side of GF. For both cases, the absolute value of the relative variation of electrical resistance was increased with the bending curvature. More importantly, the relative variation of electrical resistance for double-layer GF/PDMS−PET composite can be up to six times higher than single-layer GF/PDMS composite for the same bending curvature. These observations were further supported by the principle of mechanics of material. The 3D GF/PDMS−PET composite also has higher flexibility and environment stability and can be utilized as a strain sensor with high sensitivity, which can find important applications in real-time monitoring of buildings, such as a bridge, dam, and high-speed railway.

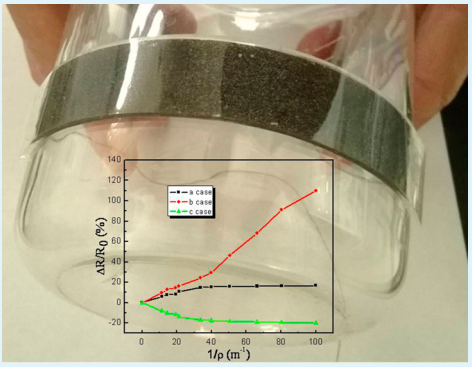

KEYWORDS: *strain sensor, three-dimensional graphene foam/poly(dimethylsiloxane) composite, bending sensitivity, flexible, environmental, principle of mechanics of material*

1. INTRODUCTION

Graphene is a two-dimensional monolayer sheet of sp^2-hybridized carbon atoms arranged in a honeycomb lattice. Since it was discovered by Geim and Novoselov in 2004,[1] it has become the focus of extensive research owing to its extraordinary structural, electrical, thermal, optical, and mechanical properties.[2−8] Due to these unique properties, graphene has great potential in fundamental research and practical applications, such as electrodes of energy storage devices,[9,10] field-effect devices,[11] chemical and biological sensors,[12,13] and fillers in conductive polymeric composites.[14] Recently, research on graphene mainly focuses on three aspects, i.e., the preparation method, properties, and applications of graphene. Since graphene properties directly determine its applications, the properties of graphene must be improved or some novel properties should be exploited for their realistic applications.

Due to the fact that the generation and control of the electrical signal are very simple and convenient, applications of graphene based on the electrical properties are much more facile compared with those based on the mechanical, thermal, and optical properties. Thus, research on the electrical properties of graphene is more important, and there have been abundant research results achieved.[15−18] The electrical properties of graphene depend not only on the preparation method of graphene but also on the stress, electric field, magnetic field, and other physical factors applied on graphene, which inevitably results in the complexity of the problem. In comparison to the electric field and magnetic field, stress can be applied to graphene more easily, and applications that relate to the stress are very universal, such as pressure sensors, ultrasonic sensors, and exploration of oil and coal.[19,20] Additionally, flexible sensors have attracted great interest due to their soft and rubbery properties and potential applications, for example, in recent years conductive polymer composites (CPCs) with two-dimensional (2D) graphene, carbon black, or carbon nanotubes as conductive fillers have been widely investigated and proposed to act as sensors for various stimulis, such as

Received: April 13, 2014
Accepted: July 29, 2014
Published: July 29, 2014

strain, pressure, and touch.[21−24] Although the effect of the stress on the electrical properties of 2D graphene has been extensively studied both theoretically and experimentally,[25−29] to date similar research about 3D graphene has been hardly reported. The 3D graphene structures, such as sponges, aerogels, and foams, have been intensively investigated due to their low mass density, large surface area, outstanding mechanical stability, and high electrical conductivity.[30−33] More recently, Z. P. Chen et al. reported that 3D graphene foam can be synthesized using the template-directed CVD method and the 3D GF consists of an interconnected flexible network of graphene as the fast transport channel of charge carriers for high electrical conductivity, which makes the 3D GF possible to be used as flexible, foldable, and stretchable conductors.[30] However, research on the electrical properties of the 3D GF under bending stress is rather scarce. To our knowledge, this is the first time we systematically report on the effect of bending stress on the electrical properties of the 3D GF.

In this paper, we fabricated a 3D GF/PDMS composite by infiltrating PDMS into GF, which was synthesized by CVD with nickel foam as a template. The effect of the bending stress on the electrical properties of the GF/PDMS composite was systematically studied, indicating the resistance of the GF/PDMS composite was increased with the bending curvature. Furthermore, a novel method to improve the stress sensitivity of the GF/PDMS composite was also proposed by introducing a thin layer of PET as substrate to form double-layer GF/PDMS−PET composite, whose physical mechanism has been well interpreted with the principle of mechanics of material. The 3D GF/PDMS−PET composite also has higher flexibility and environment stability and can be used as strain sensor, which can find important applications in real-time monitoring of buildings, such as a bridge, dam, and high-speed railway.

2. EXPERIMENTAL DETAILS

2.1. Synthesis of 3D GF/PDMS Composite and 3D GF/PDMS−PET Composite. Details of the synthesis process of the 3D GF/PDMS−PET composite is illustrated in Figure 1. In brief, nickel

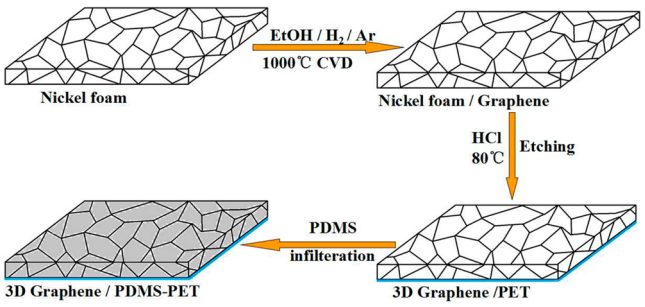

Figure 1. Schematic of the fabrication of the 3D GF/PDMS−PET composite.

foam, a porous structure with an interconnected 3D scaffold of nickel, was first used as a template for growth of GF.[34−36] During this process, the nickel foam was cut into a rectangle with a size of 20 × 2 cm^2 and then placed into a quartz tubular furnace and heated to 1000 °C at a heating rate of 50 °C/min. In order to make the surface of nickel foam clean, the nickel foam should be kept at 1000 °C about 10 min for pretreatment. Then, the ethanol as carbon source was passed into the tubular furnace under a mixed gas of H_2 and Ar as the carrier gas, in which the gas flow of H_2 and Ar was controlled at 25 and 50 sccm, respectively. The whole growth process was controlled under standard atmospheric pressure. After 20 min of growth, the tubular furnace was immediately closed and cooled down to room temperature. In the next step, nickel substrates were etched by HCl solution (10%) at 80 °C overnight to get 3D self-standing GF. Subsequently, the GF was placed on a thin PET film, and two metal wires were attached to the both ends of the GF using conductive silver adhesives. After drying of the conductive silver adhesives, the GF was integrated with PDMS in a 5:1 (base:curing agent) ratio to get double-layer 3D GF/PDMS−PET composite. To make a contrast with double-layer 3D GF/PDMS−PET composite, we also fabricate a single-layer 3D GF/PDMS composite without PET substrate under the same conditions.

2.2. Characterization. Surface morphologies of 3D GF were characterized by scanning electron microscopy (SEM, JEOL, JSM-6700F), and their Raman spectra (excited at 514 nm) were obtained by a confocal Raman microscope (CRM200, WITec).

2.3. Electrical Measurements. The electrical resistance of the 3D GF/PDMS composite and 3D GF/PDMS−PET composite was measured in a Wheastone bridge. The detailed testing circuit is shown in Figure 2a, where R_1 and R_2 are two resistors, R_3 is a variable resistance box, and G is a pointer galvanometer. In the testing, the resistance of R_1 is setted to be equal to R_2; thus, the pointer of G would point to the zero position when the resistance of the sample is equal to that of R_3. The sample used in the experiment was cut into a rectangular plate with a size of 20 × 2 × 0.1 cm^3. In order to form a closed loop, the wires were connected with the sample at both ends. The resistance of the sample under different bending curvature was tested. As an example, an optical image of the 3D GF/PDMS−PET composite bended on a beaker is shown in Figure 2b. Shown in the bottom inset of Figure 2b is the cross-sectional optical microscopy image of the 3D GF/PDMS in which the pale region indicating the transparent PDMS forms a large contrast relative to the graphene scaffolds.

3. RESULTS AND DISCUSSION

Figure 2c presents the scanning electron microscopy (SEM) image of the 3D graphene foam, which shows the 3D GF exhibits a well-defined macroporous structure with a pore diameter ≈ 100−200 μm. Shown in the upper inset of Figure 2c is the higher magnified SEM image of the 3D GF, from which it can be clearly seen that the thin graphene scaffold has a smooth surface, assuming the identical surface topology as nickel substrate due to conformal CVD. The Raman spectrum of the 3D GF is shown in Figure 2d, which presents two prominent characteristic peaks at ∼1560 and ∼2700 cm^{-1}, corresponding to the G and 2D bands of graphene, respectively. The absence of a D band at ∼1350 cm^{-1} in the Raman spectrum indicates that the 3D GF is of high quality with few defects. The shape of the 2D band and the intensity ratio between the 2D and the G bands prove that the 3D GF is composed of few-layer or multilayer graphene sheets.[37] In general, the defectless, few-layer, and low intersheet junction contact resistance ensure high electrical conductivity of 3D GF.[30,31]

Figure 3 presents the plot of the relative variation of electrical resistance for single-layer 3D GF/PDMS composite and double-layer 3D GF/PDMS−PET composite as a function of bending curvature $1/\rho$, where ρ is the bend radius, the relative variation of electrical resistance is defined as $\Delta R/R_0 = (R - R_0)/R_0$, and R_0 is the resistance of the unbent sample ($\rho = 0$). There are three cases in Figure 3: case a is for single-layer 3D GF/PDMS composite, case b is for double-layer 3D GF/PDMS−PET composite when it bended to the side of PET, and case c is for double-layer 3D GF/PDMS−PET composite when it bended to the side of graphene. As can be clearly seen from Figure 3, the electrical resistance is increased with the bending curvature for cases a and b, whereas the electrical

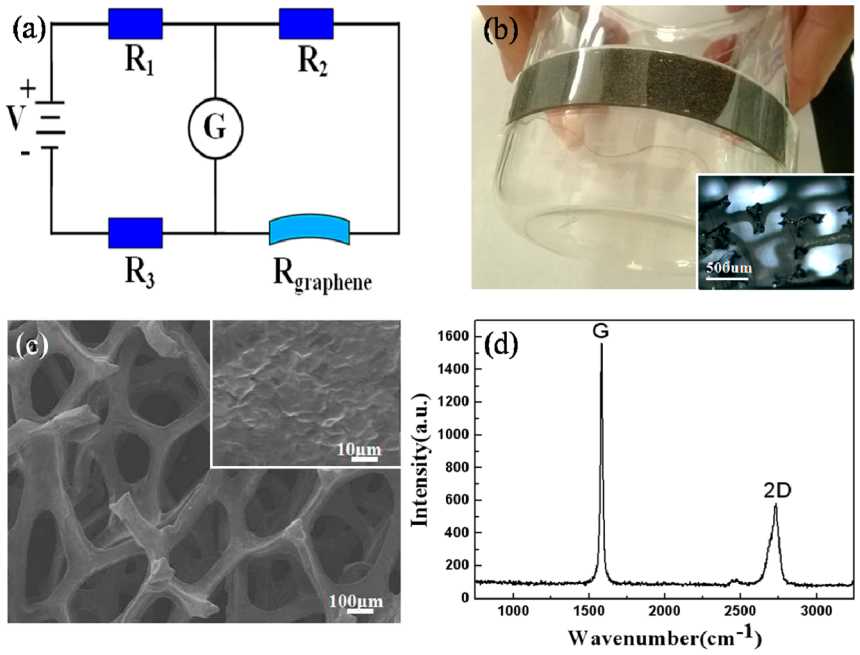

Figure 2. (a) Schematic representation of the testing circuit of the 3D GF/PDMS composite and 3D GF/PDMS−PET composite. (b) Optical image of the 3D GF/PDMS−PET composite bended on a beaker, and (bottom inset) cross-sectional optical microscopy image of the 3D GF/PDMS composite. (c and d) Characterization of the as-prepared self-standing graphene foam: (c) SEM images of the 3D graphene foam at different magnification, (d) Raman spectrum of the 3D graphene foam.

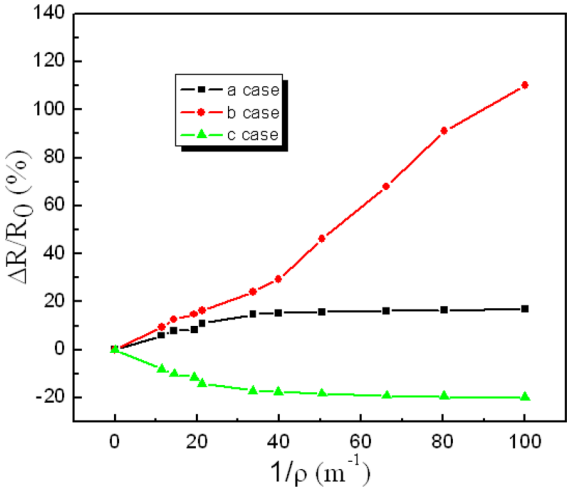

Figure 3. Plot of the relative variation of electrical resistance for single-layer 3D GF/PDMS composite and double-layer 3D GF/PDMS−PET composite as a function of bending curvature $1/\rho$, where ρ is the bend radius.

resistance is decreased with the bending curvature for case c. For the three cases, however, the absolute value of the relative variation of electrical resistance is increased with the bending curvature. More importantly, it is found that the relative variation of electrical resistance of double-layer GF/PDMS−PET composite can reach six times higher than that of single-layer GF/PDMS composite for the same bending curvature, that is, the bending sensitivity of double-layer GF/PDMS−PET composite is much higher than that of single-layer GF/PDMS composite. The results can be well interpreted with the principle of mechanics of material.[38]

When a sheet is bended, the distribution of the stress inside the sheet can be analyzed using the principle of mechanics of the material.[38] There exists a zero stress line (also referred to as the neutral axis) in a sheet under bending the sheet downward, below which all fibers are in a tension state and above which they are in a compression state. The transition from tension to compression due to bending occurs on the neutral axis, whose position in the sheet depends on the properties of materials.[38] Figure 4a and 4b shows the position of the neutral axis (marked

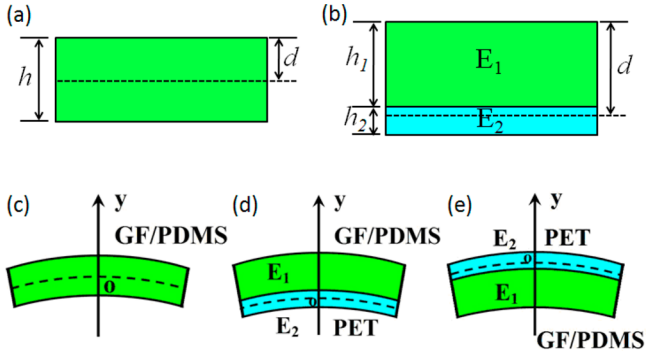

Figure 4. Schematic of the position of the neutral axis (dashed line) for single-layer sheet (a) and double-layer sheet (b). (c−e) Schematic of the position of the neutral axis for the three cases: (a) single-layer 3D GF/PDMS composite, (b) double-layer 3D GF/PDMS−PET composite when it bended to the side of PET, (c) double-layer 3D GF/PDMS−PET composite when it bended to the side of graphene.

using a dashed line) for a single-layer sheet and double-layer sheet, respectively, where h is the thickness of the sheet and d is the distance between the top surface of the sheet and the position of the neutral axis. For a single-layer sheet, the neutral axis is at the middle of the sheet, $d = h/2$, as shown in Figure 4a. However, it is different for a double-layer sheet composed of two materials with different Young's modulus. According to the principle of mechanics of the material,[38] the position of the

dx.doi.org/10.1021/am502208g | ACS Appl. Mater. Interfaces 2014, 6, 13455−13460

neutral axis in the double-layer sheet with two different materials can be given by

$$d = \frac{h_1 \times \frac{h_1}{2} + \eta h_2\left(h_1 + \frac{h_2}{2}\right)}{h_1 + \eta h_2} \quad (1)$$

where $\eta = E_2/E_1$, E_1 and E_2 are the Young's modulus of two different materials, and h_1 and h_2 are the thicknesses of two different materials, respectively, as shown in Figure 4b.

The distribution of the stress in a sheet is given by eq 2, where y is the distance between the point analyzed and the neutral axis, $\sigma(y)$ is the stress at the point analyzed, ρ is the bending radius, and E is the Young's modulus of the position at the point analyzed. For a sheet bent downward, if the point analyzed is above the neutral axis, y is positive and the stress at this point is tensile stress. On the contrary, if the point analyzed is below the neutral axis, y is negative and the stress at this point is compressive stress

$$\sigma(y) = E\frac{y}{\rho} \quad (2)$$

Figure 4c–e shows the schematic of the position of the neutral axis for the three cases a, b, and c in Figure 3. For single-layer 3D GF/PDMS composite (case a), the neutral axis is in the middle of the sheet, as shown in Figure 4a. In this case, a part of graphene is under tensile stress while another part is under compressive stress during the bending process. The effect of the compressive stress and tensile stress on the electrical properties of the graphene is just the opposite, thus resulting in the lower relative variation of electrical resistance compared to cases b and c, as shown in Figure 3. In order to improve the bending sensitivity of the GF/PDMS composite, graphene should be wholly under tensile stress or compressive stress. One medium layer should be attached to the single-layer 3D GF/PDMS composite, which could make the position of the neutral axis move away from the graphene instead of in the middle of graphene layer. Therefore, a PET layer with a thickness of 0.01 cm was chosen as the medium layer, which has greater Young's modulus compared with PDMS. Usually the Young's modulus of PDMS is about 5–10 MPa, while the Young's modulus of PET is about 3700 MPa. According to eq 1, d = 1.03 mm can be obtained, which results in the position of the neutral axis moving into the PET layer (see Figure 4d and 4e). For double-layer 3D GF/PDMS–PET composite when it bended to the side of PET (case b) the electrical resistance of graphene will increase during the tensile stress of graphene[30] and its conductivity becomes poor, as shown in Figure 3. As for double-layer 3D GF/PDMS–PET composite when it bended to the side of graphene (case c), the electrical resistance of graphene will decrease during the compressive stress of graphene and its conductivity becomes good, as shown in Figure 3. The effect of the tensile stress on the electrical resistance variation is greater than the compressive stress. Therefore, the relative variation of electrical resistance is largest for case b, which further proves the highest bending sensitivity for double-layer GF/PDMS–PET composite when it bended to the PET side, as shown in Figure 3.

We further investigated the electrical and bending properties of double-layer GF/PDMS–PET composite when it bended to the PET side by measuring its electrical resistance as a function of bend cycles. Figure 5a shows the results at the bending curvature $1/\rho$ = 39.84 m^{-1}. It can be clearly seen that the resistance of the composite increases with bending and

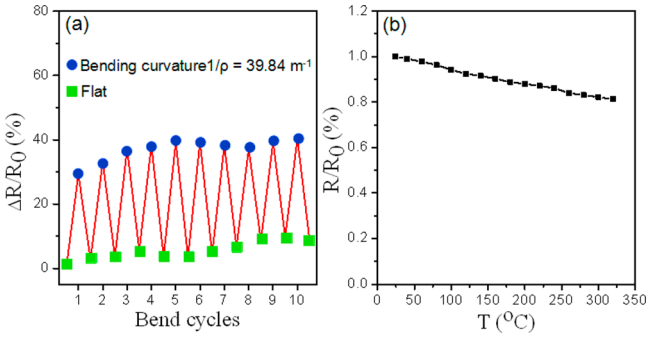

Figure 5. (a) Electrical resistance variation of the GF/PDMS–PET composite when it bended to the PET side with a bending curvature $1/\rho$ = 39.84 m^{-1} and then releasing for each cycle. (b) Electrical resistance variation of the 3D graphene foam as a function of temperature.

decreases with releasing, and its resistance change is quite stable with increasing the cycle of bending–releasing, indicating that the double-layer GF/PDMS–PET composite has excellent electromechanical stability. Besides, we also investigated the effect of the temperature on the electrical properties of the 3D graphene foam. The electrical resistance of the 3D GF as a function of temperature is shown in Figure 5b, which shows that the resistance of the 3D GF decreases slowly with an increase in temperature and exhibits an almost horizontal line in relation with the temperature, especially for the common environmental temperature. Therefore, the 3D GF has higher environment stability and can be widely utilized in our daily life as a stress sensor.

It is noted here that for realistic application of the GF/PDMS composites as a strain sensor it is very necessary to achieve detailed information regarding this kind of sensor, such as gauge factor, strain level, and response time. Figure 6 presents

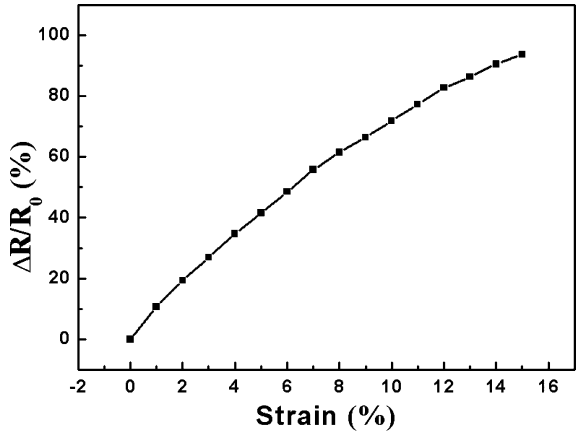

Figure 6. Polt of electrical resistance variation of the GF/PDMS composite as a function of applied strain.

the plot of the electrical resistance variation of the GF/PDMS composite as a function of applied strain. As can be seen from Figure 6, the average gauge factor of the GF/PDMS composite sensor can be estimated to be about 6.24, a value usually higher than the CPCs with 2D graphene or carbon nanotubes as conductive fillers,[39,40] which most likely arises from the low mass density, large surface area, outstanding mechanical stability, and ultrahigh conductivity for the 3D GF.[30−33] Since the GF/PDMS composites are composites, the strain level of

the GF/PDMS composite sensor should depend on the properties of both PDMS and GF. Considering the Young's modulus of PDMS (about 5−10 MPa) and the composites allowed strain, the strain level of the GF/PDMS composite sensor can be estimated to be about 3 MPa. As for the response time of the GF/PDMS composite sensor, which should mainly depend on the response time of PDMS, both the sample size and the deformation degree have an effect on the response time of the GF/PDMS composite sensor. Due to the fact that the response time of PDMS is usually longer, which can reach second order at larger sample size and larger deformation conditions, the GF/PDMS composite sensor is suitable for static stress measurement and not suitable for transient stress measurement. However, provided we choose materials with shorter response time, such as using PMMA instead of PDMS, the response time can be reduced but the soft and rubbery properties of PMMA are far lower than PDMS.

4. CONCLUSIONS

We investigated the effect of the bending stress on the electrical properties of 3D GF/PDMS composite and 3D GF/PDMS−PET composite. The results showed that the bending sensitivity of single-layer GF/PDMS composite is far less than that of double-layer GF/PDMS−PET composite. According to the principle of mechanics of the material, for single-layer GF/PDMS composite a part of graphene suffers from the compressive stress while another part suffers from the tensile stress when it is bended. The effect of the compressive stress and the tensile stress on the electrical properties of the graphene is just the opposite, thus resulting in the lower relative variation of electrical resistance. For double-layer GF/PDMS−PET composite, however, graphene can be wholly under tension stress or compression stress by introducing a high Young's modulus PET layer as substrate, whose thickness is far less than the thickness of GF/PDMS composite. Therefore, the bending sensitivity of double-layer GF/PDMS−PET composite is much higher than that of single-layer GF/PDMS composite. The 3D GF/PDMS−PET composite plate also has higher flexibility and environment stability and can be used as a strain sensor with high sensitivity, which can find important applications in real-time monitoring of buildings, such as a bridge, dam, and high-speed railway.

AUTHOR INFORMATION

Corresponding Author

*E-mail: jchen@njupt.edu.cn.

Notes

The authors declare no competing financial interest.

ACKNOWLEDGMENTS

The authors acknowledge financial support from the National Natural Science Foundation of China (Grant nos. 11304159, 11326225, 61101012, 11104032), the Specialized Research Fund for the Doctoral Program of Higher Education of China (Grant no. 20133223120006), the Scientific Research Foundation of Nanjing University of Posts and Telecommunications (Grant no. NY213023), and the Graduate Research Innovation Foundation of Nanjing University (Grant no. 2013CL10).

REFERENCES

(1) Novoselov, K. S.; Geim, A. K.; Morozov, S. V.; Jiang, D.; Zhang, Y.; Dubonos, S. V.; Grigorieva, I. V.; Firsov, A. A. Electric Field Effect in Atomically Thin Carbon Films. *Science* **2004**, *306*, 666−9.

(2) Dong, X. C.; Li, B.; Wei, A.; Cao, X. H.; Chan-Park, M. B.; Zhang, H.; Li, L. J.; Huang, W.; Chen, P. One-Step Growth of Graphene-Carbon Nanotube Hybrid Materials by Chemical Vapor Deposition. *Carbon* **2011**, *49*, 2944−2949.

(3) Zhang, Y. B.; Tan, Y. W.; Stormer, H. L.; Kim, P. Experimental Observation of the Quantum Hall Effect and Berry's Phase in Graphene. *Nature* **2005**, *438*, 201−4.

(4) Han, M. Y.; Özyilmaz, B.; Zhang, Y. B.; Kim, P. Energy Band Gap Engineering of Graphene Nanoribbons. *Phys. Rev. Lett.* **2007**, *98*, 206805−206808.

(5) Bolotin, K. I.; Sikes, K. J.; Jiang, Z.; Klima, M.; Fudenberg, G.; Hone, J.; Kim, P.; Stormer, H. L. Ultrahigh Electron Mobility in Suspended Graphene. *Solid State Commun.* **2008**, *146*, 351−355.

(6) Balandin, A. A.; Ghosh, S.; Bao, W. Z.; Calizo, I.; Teweldebrhan, D.; Miao, F.; Lau, C. N. Superior Thermal Conductivity of Single-Layer Graphene. *Nano Lett.* **2008**, *8*, 902−907.

(7) Bunch, J. S.; van der Zande, A. M.; Verbridge, S. S.; Frank, I. W.; Tanenbaum, D. M.; Parpia, J. M.; Craighead, H. G.; McEuen, P. L. Electromechanical Resonators from Graphene Sheets. *Science* **2008**, *315*, 490−493.

(8) Lee, C. G.; Wei, X. D.; Kysar, J. W.; Hone, J. Measurement of the Elastic Properties and Intrinsic Strength of Monolayer Graphene. *Science* **2008**, *321*, 385−388.

(9) Dong, X. C.; Cao, Y. F.; Wang, J.; Chan-Park, M. B.; Wang, L. H.; Huang, W.; Chen, P. Hybrid Structure of Zinc Oxide Nanorods and Three Dimensional Graphene Foam for Supercapacitor and Electrochemical Sensor Applications. *RSC Adv.* **2012**, *2*, 4364−4369.

(10) Wang, Y.; Shi, Z. Q.; Huang, Y.; Ma, Y. F.; Wang, C. Y.; Chen, M. M.; Chen, Y. S. Supercapacitor Devices Based on Graphene Materials. *J. Phys. Chem. C* **2009**, *113*, 13103−13107.

(11) Gilje, S.; Han, S.; Wang, M. S.; Wang, K. L.; Kaner, R. B. A Chemical Route to Graphene for Device Applications. *Nano Lett.* **2007**, *7*, 3394−8.

(12) Fowler, J. D.; Allen, M. J.; Tung, V. C.; Yang, Y.; Kaner, R. B.; Weiller, B. H. Practical Chemical Sensors from Chemically Derived Graphene. *ACS Nano* **2009**, *3*, 301−306.

(13) Dong, X. C.; Long, Q.; Wang, J.; Chan-Park, M. B.; Huang, Y. X.; Huang, W.; Chen, P. A Graphene Nanoribbon Network and Its Biosensing Application. *Nanoscale* **2011**, *3*, 5156−5160.

(14) Ramanathan, T.; Abdala, A. A.; Stankovich, S.; Dikin, D. A.; Herrera-Alonso, M.; Piner, R. D.; Adamson, D. H.; Schniepp, H. C.; Chen, X.; Ruoff, R. S.; Nguyen, S. T.; Aksay, I. A.; Prud'Homme, R. K.; Brinson, L. C. Functionalized Graphene Sheets for Polymer Nanocomposites. *Nat. Nanotechnol.* **2008**, *3*, 327−331.

(15) Yuan, J. T.; Ma, L. P.; Pei, S. F.; Du, J. H.; Su, Y.; Ren, W. C.; Cheng, H. M. Tuning the Electrical and Optical Properties of Graphene by Ozone Treatment for Patterning Monolithic Transparent Electrodes. *ACS Nano* **2013**, *7*, 4233−4241.

(16) Song, W. L.; Cao, M. S.; Lu, M. M.; Bi, S.; Wang, C. Y.; Liu, J.; Yuan, J.; Fan, L. Z. Flexible Graphene/Polymer Composite Films in Sandwich Structures for Effective Electromagnetic Interference Shielding. *Carbon* **2014**, *66*, 67−76.

(17) Shiu, H. W.; Chang, L. Y.; Lee, K. H.; Chen, H. Y.; Gwo, S.; Chen, C. H. Graphene as Tunable Transparent Electrode Material on GaN: Layer-Number-Dependent Optical and Electrical Properties. *Appl. Phys. Lett.* **2013**, *103*, 081604−081607.

(18) Dong, X. C.; Long, Q.; Wei, A.; Zhang, W. J.; Li, L. J.; Chen, P.; Huang, W. The Electrical Properties of Graphene Modified by Bromophenyl Groups Derived from a Diazonium Compound. *Carbon* **2012**, *50*, 1517−1522.

(19) Zhu, S. E.; Ghatkesar, M. K.; Zhang, C.; Janssen, G. C. A. M. Graphene Based Piezoresistive Pressure Sensor. *Appl. Phys. Lett.* **2013**, *102*, 161904−161907.

(20) Ma, J.; Xuan, H. F.; Ho, H. L.; Jin, W.; Yang, Y. H.; Fan, S. C. Fiber-Optic Fabry–Pérot Acoustic Sensor With Multilayer Graphene Diaphragm. *IEEE Photon. Technol. Lett.* **2013**, *25*, 932–935.
(21) Robert, C.; Feller, J. F.; Castro, M. Sensing Skin for Strain Monitoring Made of PC–CNT Conductive Polymer Nanocomposite Sprayed Layer by Layer. *ACS Appl. Mater. Interfaces* **2012**, *4*, 3508–3516.
(22) Segev-Bar, M.; Landman, A.; Nir-Shapira, M.; Shuster, G.; Haick, H. Tunable Touch Sensor and Combined Sensing Platform: Toward Nanoparticle-based Electronic Skin. *ACS Appl. Mater. Interfaces* **2013**, *5*, 5531–5541.
(23) Lin, L.; Liu, S. Y.; Zhang, Q.; Li, X. Y.; Ji, M. Z.; Deng, H.; Fu, Q. Towards Tunable Sensitivity of Electrical Property to Strain for Conductive Polymer Composites Based on Thermoplastic Elastomer. *ACS Appl. Mater. Interfaces* **2013**, *5*, 5815–5824.
(24) Cattin, C.; Hubert, P. Piezoresistance in Polymer Nanocomposites with High Aspect Ratio Particles. *ACS Appl. Mater. Interfaces* **2014**, *6*, 1804–1811.
(25) Bissett, M. A.; Tsuji, M.; Ago, H. Mechanical Strain of Chemically Functionalized Chemical Vapor Deposition Grown Graphene. *J. Phys. Chem. C* **2013**, *117*, 3152–3159.
(26) Smith, A. D.; Niklaus, F.; Paussa, A.; Vaziri, S.; Fischer, A. C.; Sterner, M.; Forsberg, F.; Delin, A.; Esseni, D.; Palestri, P.; O, M. Electromechanical Piezoresistive Sensing in Suspended Graphene Membranes. *Nano Lett.* **2013**, *13*, 3237–3242.
(27) Hajgató, B.; Güryel, S.; Dauphin, Y.; Blairon, J. M.; Miltner, H. E.; Van Lier, G.; Proft, F. D.; Geerlings, P. Theoretical Investigation of the Intrinsic Mechanical Properties of Single- and Double-Layer Graphene. *J. Phys. Chem. C* **2012**, *116*, 22608–22618.
(28) Yu, T.; Ni, Z. H.; Du, C. L.; You, Y. M.; Wang, Y. Y.; Shen, Z. X. Raman Mapping Investigation of Graphene on Transparent Flexible Substrate: The Strain Effect. *J. Phys. Chem. C* **2008**, *112*, 12602–12605.
(29) Wang, Y.; Yang, R.; Shi, Z. W.; Zhang, L. C.; Shi, D. X.; Wang, E.; Zhang, G. Y. Super-Elastic Graphene Ripples for Flexible Strain Sensors. *ACS Nano* **2011**, *5*, 3645–50.
(30) Chen, Z. P.; Ren, W. C.; Gao, L. B.; Liu, B. L.; Pei, S. F.; Cheng, H. M. Three-Dimensional Flexible and Conductive Interconnected Graphene Networks Grown by Chemical Vapour Deposition. *Nat. Mater.* **2011**, *10*, 424–428.
(31) Dong, X. C.; Wang, X. W.; Wang, L. H.; Song, H.; Zhang, H.; Huang, W.; Chen, P. 3D Graphene Foam as a Monolithic and Macroporous Carbon Electrode for Electrochemical Sensing. *ACS Appl. Mater. Interfaces* **2012**, *4*, 3129–3133.
(32) Yavari, F.; Chen, Z. P.; Thomas, A. V.; Ren, W. C.; Cheng, H. M.; Koratkar, N. High Sensitivity Gas Detection Using a Macroscopic Three-Dimensional Graphene Foam Network. *Sci. Rep.* **2011**, *1*, 166–5.
(33) Wu, Z. S.; Sun, Y.; Tan, Y. Z.; Yang, S.; Feng, X.; Müllen, K. Three-Dimensional Graphene-Based Macro- and Mesoporous Frameworks for High-Performance Electrochemical Capacitive Energy Storage. *J. Am. Chem. Soc.* **2012**, *134*, 19532–5.
(34) Dong, X. C.; Wang, J. X.; Wang, J.; Chan-Park, M. B.; Li, X. G.; Wang, L. H.; Huang, W.; Chen, P. Supercapacitor Electrode Based on Three-Dimensional Graphene-Polyaniline Hybrid. *Mater. Chem. Phys.* **2012**, *134*, 576–580.
(35) Dong, X. C.; Wang, X. W.; Wang, J.; Song, H.; Lia, X. G.; Wang, L. H.; Chan-Park, M. B.; Li, C. M.; Chen, P. Synthesis of A MnO_2-Graphene Foam Hybrid with Controlled MnO_2 Particle Shape and Its Use as A Supercapacitor Electrode. *Carbon* **2012**, *50*, 4865–4870.
(36) Maiyalagan, T.; Dong, X. C.; Chen, P.; Wang, X. Electrodeposited Pt on Three-Dimensional Interconnected Graphene as A Free-Standing Electrode for Fuel Cell Application. *J. Mater. Chem.* **2012**, *22*, 5286–4290.
(37) Ferrari, A. C.; Meyer, J. C.; Scardaci, V.; Casiraghi, C.; Lazzeri, M.; Mauri, F.; Piscanec, S.; Jiang, D.; Novoselov, K. S.; Roth, S.; Geim, A. K. Raman Spectrum of Graphene and Graphene Layers. *Phys. Rev. Lett.* **2006**, *97*, 187401–187404.
(38) Hibbeler, R. C. *Mechanics of Materials*, 9th ed.; Prentice Hall, Inc.: Upper Saddle River, NJ, 2013.
(39) Wang, Y.; Yang, R.; Shi, Z. W.; Zhang, L. C.; Shi, D. X.; Wang, E. E.; Zhang, G. Y. Super-Elastic Graphene Ripples for Flexible Strain Sensors. *ACS Nano* **2011**, *5*, 3645–3650.
(40) Khang, D. Y.; Xiao, J. L.; Kocabas, C.; MacLaren, S.; Banks, T.; Jiang, H. Q.; Y. Huang, Y. G.; Rogers, J. A. Molecular Scale Buckling Mechanics in Individual Aligned Single-Wall Carbon Nanotubes on Elastomeric Substrates. *Nano Lett.* **2008**, *8*, 124–130.